An integrated design and fabrication strategy for entirely soft, autonomous robots

An Integrated Design and Fabrication Strategy for Entirely Soft, Autonomous Robots

Michael Wehner[*,1,2], Ryan L. Truby[*,1,2], Daniel J. Fitzgerald[1,2], Bobak Mosadegh[3,4], George M. Whitesides[2,5], Jennifer A. Lewis[1,2,**], Robert J. Wood[1,2,**]

[1]John A. Paulson School of Engineering and Applied Sciences, Harvard University, Cambridge, Massachusetts, 02138 USA. [2]Wyss Institute for Biologically Inspired Engineering, Harvard University, Cambridge, Massachusetts, 02138 USA. [3]Dalio Institute of Cardiovascular Imaging, Weill Cornell Medicine and New York Presbyterian Hospital, New York, New York, 10021 USA [4]Department of Radiology, Weill Cornell Medicine, New York, New York, 10021 USA. [5]Department of Chemistry and Chemical Biology, Harvard University, Cambridge, Massachusetts, 02138 USA.

[*]These authors contributed equally to this work.
[**]Corresponding authors

Soft robots possess many attributes that are difficult, if not impossible, to realize with conventional robots composed of rigid materials.[1,2] Yet, despite recent advances, soft robots still remain tethered to hard robotic control systems and power sources.[3–12] New strategies for creating completely soft robots, including soft analogs of these crucial components, are needed to realize their full potential. Here, we report the first untethered operation of a robot comprised solely of soft materials. The robot is controlled with microfluidic logic[13] that autonomously regulates the catalytic decomposition of an on-board monopropellant fuel supply. Gas generated from fuel decomposition inflates fluidic networks downstream of the reaction sites, resulting in actuation.[14] The robot's body and microfluidic logic are fabricated by molding and soft lithography, respectively, while the pneumatic actuator networks, on-board fuel reservoirs and catalytic reaction chambers needed for movement are patterned within the body via a multi-material, embedded 3D printing technique.[15,16] The relevant length scales of fluidic and elastomeric architectures required for function spanned several orders of magnitude. Our integrated design and rapid fabrication

approach enables the programmable assembly of multiple materials within this architecture, laying the foundation for completely soft, autonomous robots.

Soft robotics is a nascent field that aims to provide safer, more robust robots that interact with humans and adapt to natural environments better than their rigid counterparts. Unlike conventional robots composed of rigid materials, soft robots based on hydrogels,[17,18] electroactive polymers,[19] granular media,[20] and elastomers[5,21] exhibit elastic moduli ranging from 100kPa to 1MPa,[1] are physically resiliant,[22,23] and have the ability to passively adapt to their environment.[1,2] Molded and laminated elastomers with embedded pneumatic networks are widely used materials in soft robotics.[1,21] Actuation of these elastomeric composites occurs when interconnected channels comprising the pneumatic network are inflated with incompressible fluids or gases supplied via tethered pressure sources.[1] Robotic end effectors with bioinspired[7] and rapid[24] actuation, deployable crawlers[3,10] and swimmers[11] with complex body motions, and robust jumpers[6,12] have been developed based on this design strategy. However, in each case, these robots are either tethered to or carry rigid systems for power and control, yielding hybrid soft-rigid systems.[4,8,10–12]

Creating a new class of fully soft, autonomous robots[25] is a grand challenge, as it requires soft analogs of the control and power hardware currently used. Recently, monopropellant fuels have been suggested as a promising fuel source for pneumatically actuated soft robots.[4,14] Their rapid decomposition into gas upon exposure to a catalyst offers a strategy for powering soft robotic systems that obviates the need for batteries or external power sources. Here, we report a method for creating a completely soft, pneumatic robot, the “octobot”, with eight arms that are powered by monopropellant decomposition. To accomplish this, we use microfluidic logic[13] as a soft controller and multi-material, embedded 3D (EMB3D) printing method to fabricate

pneumatic networks within a molded elastomeric, robot body. Our hybrid assembly approach allows one to seamlessly integrate soft lithography, molding, and 3D printing to rapidly and programmably fabricate myriad materials and functional elements in form factors required for autonomous, untethered operation of a soft robot.

To fabricate an octobot, we first micro-mold[13,26] the soft controller that houses the microfluidic logic necessary for controlling fuel decomposition (Figure 1a). The soft controller is placed into a mold partially filled by hyperelastic layers needed for actuation (Figure 1b). Matrix materials are then poured into the mold (Figure 1c), and the remaining soft robot features are EMB3D printed into the molded matrix (Figure 1d, 1e, Supporting Video 1). After the matrix materials are crosslinked, the aqueous fugitive inks "auto-evacuate" at elevated temperature as water evaporates from the inks and diffuses through the matrix, leaving behind an open network of channels that are interfaced with the soft controller (Figure 1f). Octobot fabrication is completed upon removal of excess matrix material (Figure 1g). A more detailed description of this multi-step assembly process is provided in Extended Data Figure 1.

By combining micro-molding with EMB3D printing, we rapidly patterned the required mesofluidic networks by extruding sacrificial inks through fine nozzles that are embedded within the uncured elastomer matrices. To self-heal crevices that form within the "body" matrix as the nozzle is translated during the printing process, we created a new elastomeric material that exhibits thixotropic behavior[27] (Extended Data Figure S2a). When completely restructured or at rest, this matrix behaves like a Herschel-Bulkley fluid, i.e., it exhibits both shear-thinning behavior (Extended Data Figure 2b), and a shear yield-stress (Extended Data Figure 2c). These properties ensure that the extruded inks remain in place within the matrix.[15,16] However, upon yielding, the body matrix readily flows (Extended Data Figure 2c) into any crevices formed. The

body matrix restructures with time, ultimately recovering its original viscoelasticity (Extended Data Figure 3), which ensures that EMB3D printing can be repeated later in the same matrix region. We also created a "fuel reservoir" elastomeric matrix, into which fuel reservoir channels are printed. Both the body and fuel reservoir matrices are crosslinked within the mold after printing is completed.

To create the fuel reservoirs, catalytic reaction chambers, actuator networks, and vent orifices, two hydrogel-based inks (fugitive and catalytic) are printed into the molded matrix materials (Figure 2a). These printed features are interfaced with each other as well as the soft controller through the use of "fugitive plugs" introduced at the controller's inlets prior to filling the mold with the matrix materials. The fugitive ink is composed of an aqueous, poly(ethylene oxide)-*b*-poly(propylene oxide)-*b*-poly(ethylene oxide) triblock copolymer (Pluronic F127) gel.[15,28] The catalytic ink contains platinum particles (Supporting Video 2) suspended in a mixture of Pluronic F127-diacrylate (F127-DA) and poly(ethylene glycol) diacrylate (PEG-DA) that is photocrosslinked after printing. The rheological properties of both inks are specifically tailored for EMB3D printing[15,16] (Figure 2b, Extended Data Figure 4). The printed features produced from both inks can be changed "on-the-fly" by varying the print speed (Figure 2c). Typically, this fugitive ink must be removed or "evacuated" after printing to yield open channels.[15,28] However, we find that the fugitive ink composed of pure Pluronic F127 can be auto-evacuated by heating the printed features within the crosslinked, silicone-based matrices at 90˚C[29] (Figure 2d, Extended Data Figure 5). As water evaporation ensues, the triblock copolymer species either form a thin coating at the matrix-open channel interface or they may partially diffuse into the matrix. The fugitive plugs within the soft controller's inlets also undergo this auto-evacuation process, facilitating connectivity between the microfluidic logic

and all printed mesofluidic components (Extended Data Figure 6). By contrast, the catalytic ink is crosslinked in place after printing yielding a Pt-laden plug within the matrix (Figure 2e).

To achieve the desired autonomous function, we incorporated a soft, microfluidic controller within the octobot (Figure 3a). The control system is roughly divided into four sections, upstream (liquid fuel storage), oscillator (liquid fuel regulation), reaction chamber (decomposition into pressurized gas), and downstream (gas distribution for actuation and venting). Upstream, 0.5 mL of fuel is infused via a syringe pump into each of two fuel reservoirs printed into the hyperelastic matrix. Upstream check valves in the soft controller prevent fuel from flowing back out the fuel inlets. The fuel reservoirs expand elastically to a pressure of approximately 50 kPa, forcing fuel into the oscillator. The oscillator includes a system of pinch and check valves based on prior designs,[13] which convert pressurized fuel inflow into alternating fuel outflow. With one channel temporarily occluded, fuel from the other channel flows from the soft controller's outlets into the Pt laden reaction chambers, where it rapidly decomposes. The resulting pressurized gas, prevented from returning to the soft controller via downstream check valves, flows into one of the downstream mesofluidic networks comprised of four actuators and one orifice. The supplied pressure deflects the actuators and exhausts to atmosphere through the vent orifice. Thus, for robust actuation and timely venting, a balance must be reached between supply gas flow, actuation pressure, and exhaust rate. These subcomponents operate based on the interaction and timing of the local pressures, similar in concept to an electrical oscillator (Figure 3b). Upon successful venting, the fuel flow into one reaction chamber stops and flow to the other begins, initiating a similar sequence in the other downstream catalytic chamber and actuator network (Figure 3c).

To provide an on-board power source, we used a 50 wt% aqueous hydrogen peroxide as the fuel due to its high energy density (1.44 kJ/g as compared to 0.1-0.2 kJ/g for batteries) as well as its benign decomposition byproducts. As the fuel decomposes in the presence of the platinum catalyst, the following reaction occurs $2H_2O_2$ (l) → $2H_2O$ (l,g) + O_2,(g), which results in a volumetric expansion of approximately 240 times (at ambient pressure).[14] At our operating pressure of 50 kPa gauge, an expansion of 160 times is expected. Although higher fuel concentrations would provide increased expansion and energy density, concentrations above 50 wt% drastically increase the decomposition temperature resulting in combustion of matrix materials that surround the reaction chambers. Since this monopropellant liquid fuel can be handled in small volumes and decomposes at the point of use, we can use microfluidic logic to directly handle the fuel, eliminating the need for external valves[10] to control gas at high pressure and flow rate.

The geometry of the microfluidic soft controller is designed to operate at a fuel flow rate of ~40 μL/min thereby yielding pressurized gas at a rate of ~6.4 mL/min.[13] Under these operating conditions, the theoretical runtime of 12.5 min could be achieved using a system with a fuel capacity of 1 mL. The actuators, which consist of printed bladders in contact with a lower modulus, hyperelastic elastomer layer (Figure 4a), are designed to inflate asymmetrically to generate angular displacement. Their maximum working pressure and displacement are tuned based on the thickness of the hyperelastic layer (Figure 4b, Extended Data Figure S7). If this layer is too thin, it ruptures prematurely. However, the working pressure increases with thickness. As a compromise, we selected a layer thickness of 1000 μm, as it affords consistent performance at the lowest working pressure. In parallel with the actuators, we tailored the diameter of the vent orifices by modulating print speed. Orifices roughly 75 μm in width allowed

proper actuator displacement with timely subsequent venting. The ability to rapidly pattern and adjust the geometry of these features "on-the-fly" via EMB3D printing allowed us to iterate through more than 30 designs and nearly 300 octobots to converge on an appropriate system-level architecture.

Through this iterative process, we created octobots with embedded components that work together in concert to alternate between the red and blue actuation states shown in Figure 4c. The resulting octobots operated autonomously (Figure 4d, Supplemental Video 3), cycling between actuation states for four to eight minutes. While this is less than the predicted theoretical runtime, the soft controller alternates actuation states as expected. We believe that downstream impedances arising from decomposition-actuation-venting cycles as well as the decreasing flow rate of fuel into the soft controller with time are responsible for the departure from theoretical performance.[13] Further advances in microfluidic logic design for soft robotic control will lead to longer periods of actuation cycles, account for dynamic fuel input, and also facilitate more sophisticated gait cycles that will enable true locomotion.

In summary, we have demonstrated the first untethered operation of a robot composed solely of soft materials. The coupling of monopropellant fuels and microfluidic logic allowed us to power, control, and realize autonomous operation of these pneumatically actuated systems. Through our hybrid assembly approach, we constructed both the robot body and embedded the necessary components for fuel storage, catalytic decomposition, and actuation to enable system-level function in a rapid manner. The octobot is a minimal system designed to demonstrate our integrated design and fabrication strategy, which may serve as a foundation for a new generation of completely soft, autonomous robots.

Methods

Soft Controller Fabrication

Soft controllers are fabricated from Sylgard 184 PDMS (Dow Corning Corp. Auburn. MI, USA) using soft lithography molding and bonding techniques. First, a mold was fabricated on a silicon wafer using SU-8 negative photoresist (Microchem, Corp. Westborough, MA, USA). SU-8 3050 photoresist was used to achieve 100 mm film thickness. Baking, exposing, and developing steps were performed in accordance with product specifications in the product datasheet. The completed wafer is placed in a petri dish to form a competed mold assembly.

Soft controllers consist of an upper mold, a lower mold, and an intermediate thin film. The upper and lower molds are made on one wafer to ease fabrication. PDMS is poured into the mold assembly to a height of one millimeter. Separately, PDMS is spun coat onto a wafer at 1500 rpm for 60 seconds for a film thickness of 35 mm. After curing at 90° C for 20 minutes, PDMS forms are removed from the molds, and holes are punched at all inlets and outlets. The upper layer is bonded to the wafer-adhered thin film after exposing to oxygen plasma at 35 Watts for 20 seconds in a Deiner Pico plasma system (Deiner Electronic GmbH). Holes are punched in the thin film, masks are placed as described by Mosadegh, et al.,[26] and the lower layer is bonded to the thin film using the plasma recipe above.

Ink and Matrix Materials

Two inks, a “fugitive ink” and “catalytic ink,” are formulated for EMB3D printing. The fugitive ink is prepared by adding 27 wt% gel of Pluronic F127 to ice-cold, deionized, ultra-filtrated (DIUF) water, followed by mixing in a planetary mixer for 5 min at 2000 rpm, and storing at 4˚C. The fugitive ink is not used until the Pluronic F127 completely dissolves in solution. The ink is prepared for printing by loading the solution at 4˚C in a 3 cc syringe barrel (EFD Nordson,

East Providence, RI, USA) and centrifuged at 3000 rpm for 5 min to degas. For EMB3D printing, the fugitive ink's barrel is fitted with a stainless steel nozzle (0.15 mm inner diameter, EFD Nordson).

The catalytic ink is prepared by first synthesizing and then dissolving a diacrylated Pluronic (F127-DA) at 30wt% concentration with a solution of Irgacure 2959 (at 0.5wt%, BASF) in DIUF water at 4˚C. The F127-DA is synthesized under an inert nitrogen atmosphere by first adding 400 mL of dry toluene (Sigma, St. Louis, MO, USA) to a three-neck flask fixed to a condenser with circulating cold water and magnetically stirred at 300 rpm. 70 g of Pluronic F127 (Sigma) is then dissolved in the toluene after heating the solvent to 60˚C. After the solution is allowed to cool to room temperature, triethylamine (5.6 g, Sigma) is added to the solution, followed by the drop-wise addition of acryloyl chloride (5 g, Sigma) with continued stirring, both at a molar ratio of 10:1 with the Pluronic F127. The reaction mixture is stirred overnight and maintained in the inert atmosphere. The diacrylated Pluronic F127 (F127-DA) product is then filtered from the yellow triethylammonium hydrocholoride byproduct and precipitated from the filtered solution with hexane (Sigma) at a 1:1 volume ratio. The F127-DA is obtained through a second filtration step and allowed to try in a chemical hood for at least 24 h. This protocol is adapted from Wu, et al.[15] For each gram of this base F127-DA mixture, 100 mg of PEG-DA is added, and this solution is mixed in a planetary mixer for 1 min at 2000 rpm and degassed for 3 min at 2200 rpm. This mixture is then stored in the dark at 4˚C. Finally, 5 w/w% Pt black (Sigma) is added to this base solution at 4˚C and mixed in a planetary mixer for 5 min at 2000 rpm. The Pt-filled F127-DA physically gels during mixing, facilitating loading into a UV-blocking 3cc syringe barrel (EFD Nordson) for printing. Note, this catalytic ink is freshly prepared for each print session, as the Pt black slowly crosslinked the acrylate moieties present in

the ink. After EMB3D printing, the catalytic ink is crosslinked for 15 min at 18 mW/cm^2 under a UV source (Omnicure EXFO). For EMB3D printing, the syringe barrel housing this ink is fitted with a stainless steel nozzle (0.33 mm inner diameter, EFD Nordson).

Two matrix materials are developed for fabricating fully soft robots. The first matrix, referred to as the "body matrix," is prepared by blending two silicone-based materials: Sylgard 184 and SE 1700 (Dow Corning). Sylgard 184 PDMS is used to dilute SE 1700 to achieve the desired rheological response for embedded 3D printing. After exploring several blends, we find that the optimal body matrix is composed of a 1:1 mass ratio of SE 1700 (4:1 ratio of base to hardener) and Sylgard 184 (10:1 ratio of base to hardener). This matrix is prepared by mixing the blend in a planetary mixer at 2000 rpm for 3 min with degassing at 2200 rpm for 2 min. The second matrix, referred to as the "fuel reservoir matrix," is prepared by mixing Part A Ecoflex 00-30 to Part B Ecoflex 00-30 (with 1.2 w/w% Slo-Jo Platinum Silicone Cure Retarder and 1.2 w/w% Thivex, Smooth-On Inc., Macungie, PA, USA) in a 1:1 ratio. The matrix is prepared in a planetary mixer at 2000 rpm for 1.5 min with degassing at 2200 rpm for 1 min.

Lastly, the "fugitive plug" material used to prevent ingress of the body matrix material into the soft controller is prepared prior to printing by first synthesizing and then mixing a diacrylated Pluronic material (F127-DA) (at 30 wt% in a 0.5 wt% solution of Irgacure 2959 in DI water) with F127 (at 30 wt% in DI water) at a mass ratio of 1:4. The fugitive plug is stored in the dark at 4˚C in a syringe. When used, the fugitive plug material is allowed to physically gel before it is crosslinked for 3 min at 6 mW/cm^2 under a UV source.

Rheological Characterization

All rheological measurements are carried out using a controlled-stress rheometer (DHR-3, TA Instruments, New Castle, DE, USA) equipped with a 40 mm diameter, 2˚ cone and plate

237 geometry. In all experiments, the fugitive and catalytic inks are equilibrated at room temperature
238 for 1 min before testing; the fuel reservoir and body matrix materials are equilibrated for 20 min
239 and 10 min, respectively, to simulate the times at which octobot printing began with each
240 material. Shear storage moduli are measured as a function of shear stress at a frequency of 1Hz.

241 The body matrix materials are characterized by both sweep and flow tests to determine
242 their rheological response (Extended Data Figure 2). In addition, three-phase modulus recovery
243 tests are carried out to quantify the recovery time of the body matrix stiffness after applying a
244 shear stress that exceeds the equilibrium yield stress, $\tau_{y,0}$ (Extended Data Figure 3). In the first set
245 of experiments, flow sweeps from low (10^{-2} s^{-1}) to high (10^{2} s^{-1}) shear rates are carried out and
246 immediately followed by ramp sweeps from high to low shear rates. In the latter set, of
247 experiments, shear storage (G') and loss (G'') moduli are measured during three phases of applied
248 shear stresses (at 1 Hz frequency): 1 Pa for 3 min; 100 Pa for either 1, 10, or 100s; and 1 Pa for
249 30 min. We defined their thixotropic recovery time, as the instant $G' = G''$, or when $\tan(\delta) = G''/$
250 $G' = 1$.

251 **Actuator Characterization.** Actuators are printed into special actuator characterization molds
252 by EMB3D printing and then auto-evacuate. To prepare them for characterization, they are first
253 released from mold assembly and then a 1 mm hole is created with a biopsy punch (Miltex Inc.
254 York, PA, USA), which serves as the air inlet. Finally, the actuator is pressurized slightly to
255 insure inflation. Each actuator design is tested for blocked force (i.e., the actuator is constrained
256 from deflection and resultant force is measured) and free displacement (i.e., the actuator is
257 allowed to deflect unconstrained and the total displacement is measured). For blocked force
258 characterization, individual actuators are mounted on a fixed platform beside an Instron model
259 5544 materials testing frame (Illinois Tool Works Inc., Norwood, MA, USA). The actuator is

lowered until just above the force sensor portion of the testing frame, and the actuator is plumbed with regulated compressed air. Actuators typically behave differently upon initial few actuations versus subsequent actuations due to the Mullins effect.[30] Each actuator therefore receives five "break in" cycles prior to data acquisition.

For each actuator, break in testing consists of five cycles, in which actuator air pressure is slowly (~30 sec) ramped up to the pressure set point, then slowly (~30 sec) ramped down to ambient. Pressure set point for the first cycle is P_0, and set point for all following cycles is P_1 (Table S1). Data acquisition consists of five additional cycles for each actuator, in which air pressure is cycled as above to pressure set point P_1. Air pressure and actuator force data is recorded on the Instron testing frame data acquisition system at 100 ms intervals.

For free displacement characterization, actuators are plumbed with regulated compressed air, and mounted vertically between a matte black background and a Sony NEX3 digital camera for video data acquisition. Actuators are pressurized with five break-in cycles as described above, followed by five data acquisition cycles. As above, the first break in cycle is to P_0, and all subsequent break in and data acquisition cycles are to P_1. Video data is analyzed using ImageJ image analysis platform (NIH.gov) to obtain bend angle versus pressure for each actuator.

Mold Fabrication

Octobot molds are fabricated inside a CNC machined Delrin® mold equipped with two locating pins to mount the soft controller. Their desired shape is modeled in Solidworks. A negative mold is modeled, and output in Parasolid format for file transfer. MasterCAM is used to develop all machining tool paths and to export final G-code for final fabrication. Blanks of 105 mm length were cut from black acetal (Delrin®), stock size 1x3 inch (McMaster Carr, Santa Fe Springs, CA, USA). Acetal is used due to its dimensional stability, and thick stock is chosen to

prevent warping during machining and repeated octobot curing cycles. Octobot molds are produced by CNC milling on a HAAS OM-2A vertical machining center (HAAS Automation Inc, Oxnard, CA, USA). 1 mm dowel pins are pressed into drilled holes for controller mounting.

Soft Robot Assembly

A custom-designed, multi-material 3D printer (ABL 10000, Aerotech Inc., Pittsburg, PA, USA) with four independently z-axis addressable ink reservoirs is used to pattern fugitive and catalytic inks within the octobot matrices.[28] All G-Code for printing is generated from Python-based software (MeCode, developed by J. Minardi). Prior to EMB3D printing, Ecoflex 30 (Smooth-On, Inc.) is first prepared with 1 wt% Slo-Jo and 0.25 wt% Thivex (both with respect to Part A) by mixing in a Thinky planetary mixer for 1.5 min with a 1 min degas cycle. This uncured Ecoflex 30 is cast into the actuator layers of the octobot mold and degassed in a vacuum chamber for 3 min. A glass slide is used to remove excess material and create smooth surfaces that will ultimately become the extensible layers of the actuators. The molds are then placed in a 90˚C oven for 30 min to cure the Ecoflex, removed, and trimmed of excess material as necessary.

A soft controller is then loaded onto the press-fit pins placed in the printing mold with the Kapton tape still adhered. Registration coordinates and print heights are then taken from the cured Ecoflex layers in the actuators and in all inlets of the soft controller; these are essential for EMB3D printing and provided to the custom print software. The fuel reservoir and body matrix materials are prepared as described previously. While the body matrix material is mixing, the fuel reservoir matrix is deposited in the fuel reservoir region of the printing mold and degassed for three minutes. Excess bubbles in the uncured fuel reservoir matrix are removed with a pipettor. Non-gelled, chilled fugitive plug is then filled throughout the soft controller via

injection through the inlets. While the fugitive plug is still in the liquid state, it is briefly degassed in a vacuum chamber. The fugitive plug material is then allowed to physically crosslink, excess gel is scraped from the top of the tape, the tape is removed, and the fugitive plug is photocrosslinked with a UV source at 6 mW/cm^2 for 3 min. After the gels are crosslinked, the body matrix is cast within the mold, covering the fuel reservoir matrix and the fugitive plug-filled soft controller and degassed for 1-3 min. Again, excess bubbles are removed with a pipettor, excess material is scraped off and away form the mold with a glass slide, and EMB3D printing of the fugitive and catalytic inks begins. After printing, the entire mold is cured at 18 mW/cm^2 for 15 min to crosslink the catalytic ink. The mold is then transferred to a 90˚C oven, where the matrix materials crosslink. The octobot is removed from the mold and kept at 90˚C for 4 days to facilitate auto-evacuation of the inks.

After auto-evacuation, the octobot is release cut from the surrounding matrix material using a CO_2 laser (Universal Laser Systems, Scottsdale, AZ, USA) and cleaned with isopropyl alcohol and water. Sylgard 184 PDMS (Dow Corning Corp. Auburn, MI, USA) is poured into the octobot's open cavity above the soft controller to a height of 1.5 mm and cured at 90°C for 20 min. A 1 mm biopsy punch (Militex Inc, York, PA, USA) is used to punch holes through the newly poured PDMS layer and into the fuel inlets. Dyed water is injected into these holes to inflate the fuel tanks, flow through the system, and insure proper bot function. Holes are punched in the downstream orifice features to allow the water to vent from the system.

The octobot is loaded into an acrylic tank outfitted with a backlight to highlight colored fuel as it flows through the system. Aqueous hydrogen peroxide (90 wt%, HTP grade, Peroxychem, Philadelphia, PA, USA) is diluted to 50 wt% and samples dyed red and blue are filled into two syringes prepared with this liquid fuel mixture. The syringes are loaded onto a

329 syringe pump, and connected to the octobot via 1mm diameter silicone rubber tubing. Water is
330 flowed into the acrylic tank to wash away dye in the octobot exhaust stream and drained into a
331 nearby sink. The syringe pump flows fuel at a rate of 3 mL/min (each syringe) into the octobot
332 for 10 sec. The silicone rubber tubing is removed with tweezers from the octobot, which is
333 allowed to operate untethered. The octobot alternates actuation until fuel pressure is insufficient
334 to switch the oscillator and alternating actuation ceases.

335 **Imaging and Videography**

336 Photographs and supporting videos are acquired with a digital SLR camera (Canon EOS
337 5D Mark II, Canon USA Inc) and a 4K video (Blackmagic Production 4K, Blackmagic Design,
338 Melbourne, Australia). Photos are cropped using Inkscape vector graphics editor
339 (www.inkscape.org), and video sequences are clipped from raw footage and exported using
340 iMovie (Apple Corp, Cupertino, CA, USA). All print parameter measurements and images of
341 EMB3D printed features in octobots are taken with a digital zoom microscope (VHX-2000,
342 Keyence, Japan). Their mean values and standard deviations are determined from three samples
343 printed at each print speed of interest.

344

345 **References**

346 1. Rus, D. & Tolley, M. T. Design, fabrication and control of soft robots. *Nature* **521,** 467–
347 475 (2015).
348 2. Wang, L. & Iida, F. Deformation in Soft-Matter Robotics: A Categorization and
349 Quantitative Characterization. *IEEE Robot. Autom. Mag.* **22,** 125–139 (2015).
350 3. Shepherd, R. F. *et al.* Multigait soft robot. *Proceedings of the National Academy of*
351 *Sciences* **108,** 20400–20403 (2011).

4. Onal, C. D., Chen, X., Whitesides, G. M. & Rus, D. Soft mobile robots with on-board chemical pressure generation. in *International Symposium on Robotics Research (ISRR)* 1–16 (2011).

5. Lin, H.-T., Leisk, G. G. & Trimmer, B. GoQBot: a caterpillar-inspired soft-bodied rolling robot. *Bioinspir. Biomim.* **6,** 026007 (2011).

6. Shepherd, R. F. *et al.* Using explosions to power a soft robot. *Angew. Chemie - Int. Ed.* **52,** 2892–2896 (2013).

7. Martinez, R. V. *et al.* Robotic tentacles with three-dimensional mobility based on flexible elastomers. *Adv. Mater.* **25,** 205–212 (2013).

8. Stokes, A. A., Shepherd, R. F., Morin, S. A., Ilievski, F. & Whitesides, G. M. A Hybrid Combining Hard and Soft Robots. *Soft Robot.* **1,** 70–74 (2014).

9. Mosadegh, B. *et al.* Pneumatic Networks for Soft Robotics that Actuate Rapidly. *Adv. Funct. Mater.* **24,** 2163–2170 (2014).

10. Tolley, M. T. *et al.* A Resilient, Untethered Soft Robot. *Soft Robot.* **1,** 213–223 (2014).

11. Marchese, A. D., Onal, C. D. & Rus, D. Autonomous Soft Robotic Fish Capable of Escape Maneuvers Using Fluidic Elastomer Actuators. *Soft Robot.* **1,** 75–87 (2014).

12. Bartlett, N. W. *et al.* A 3D-printed, functionally graded soft robot powered by combustion. *Science (80-.).* **349,** 161–165 (2015).

13. Mosadegh, B. *et al.* Integrated elastomeric components for autonomous regulation of sequential and oscillatory flow switching in microfluidic devices. *Nature Physics* **6,** 433–437 (2010).

14. Wehner, M. *et al.* Pneumatic Energy Sources for Autonomous and Wearable Soft Robotics. *Soft Robot.* **2,** 141031124812001 (2014).

15. Wu, W., Deconinck, A. & Lewis, J. A. Omnidirectional printing of 3D microvascular networks. *Adv. Mater.* **23,** H178–83 (2011).

16. Muth, J. T. *et al.* Embedded 3D printing of strain sensors within highly stretchable elastomers. *Adv. Mater.* **26,** 6307–6312 (2014).

17. Palleau, E., Morales, D., Dickey, M. D. & Velev, O. D. Reversible patterning and actuation of hydrogels by electrically assisted ionoprinting. *Nat. Commun.* **4,** 2257 (2013).

18. Ionov, L. Biomimetic hydrogel-based actuating systems. *Adv. Funct. Mater.* **23,** 4555–4570 (2013).

19. Anderson, I. A., Gisby, T. A., McKay, T. G., O'Brien, B. M. & Calius, E. P. Multi-functional dielectric elastomer artificial muscles for soft and smart machines. *J. Appl. Phys.* **112,** 0–20 (2012).

20. Brown, E. *et al.* Universal robotic gripper based on the jamming of granular material. *Proc. Natl. Acad. Sci.* **107,** 18809–18814 (2010).

21. Ilievski, F., Mazzeo, A. D., Shepherd, R. F., Chen, X. & Whitesides, G. M. Soft robotics for chemists. *Angew. Chemie - Int. Ed.* **50,** 1890–1895 (2011).

22. Shepherd, R. F., Stokes, A. A., Nunes, R. M. D. & Whitesides, G. M. Soft machines that are resistant to puncture and that self seal. *Adv. Mater.* **25,** 6709–6713 (2013).

23. Tolley, M. T. *et al.* A Resilient, Untethered Soft Robot. **1,** 213–223 (2014).

24. Mosadegh, B. *et al.* Pneumatic Networks for Soft Robotics that Actuate Rapidly. *Adv. Funct. Mater.* **24,** 2163–2170 (2014).

25. Whitesides, G. M. What comes next? *Lab Chip* **11,** 191–193 (2011).

26. Mosadegh, B., Tavana, H., Lesher-Perez, S. C. & Takayama, S. High-density fabrication of normally closed microfluidic valves by patterned deactivation of oxidized

polydimethylsiloxane. *Lab Chip* **11,** 738–742 (2011).

27. Barnes, H. A. Thixotropy - A review. *J. Nonnewton. Fluid Mech.* **70,** 1–33 (1997).

28. Kolesky, D. B. *et al.* 3D bioprinting of vascularized, heterogeneous cell-laden tissue constructs. *Adv. Mater.* **26,** 3124–3130 (2014).

29. Randall, G. C. & Doyle, P. S. Permeation-driven flow in poly(dimethylsiloxane) microfluidic devices. *Proc. Natl. Acad. Sci. U. S. A.* **102,** 10813–10818 (2005).

30. Mullins, L. Softening of Rubber by Deformation. *Rubber Chemistry and Technology* **42,** 339–362 (1969).

Acknowledgements

We thank David Gessel, Greg Leyh, Mark Pauline, Nicholas W. Bartlett, Mark A. Skylar-Scott, Thomas J. Ober, and Joseph T. Muth for their comments and discussions. We also thank Lori K. Sanders for assistance with photography and videography and James C. Weaver for assistance with electron microscopy. The authors gratefully acknowledge support from the National Science Foundation (Grant# DMR-1420570) and the Wyss Institute for Biologically Inspired Engineering. Any opinions, findings, and conclusions or recommendations expressed in this material are those of the authors and do not necessarily reflect the views of the National Science Foundation. R.L.T. also acknowledges support from a National Science Foundation Graduate Research Fellowship.

Author Contributions

M.W., R.L.T., J.A.L., and R.J.W. conceived the experimental work; M.W. and R.L.T. led the experiments with assistance from D.J.F. and B.M; M.W., R.L.T., J.A.L., and R.J.W. contributed to data analysis and interpretation and wrote the paper. All authors provided feedback.

421 **Author Information**

422 Reprints and permissions information is available at www.nature.com/reprints. The authors
423 declare no competing financial interests. Correspondence and requests for materials should be
424 addressed to R.J.W. (rjwood@seas.harvard.edu) and J.A.L. (jalewis@seas.harvard.edu).

Figures and Figure Legends

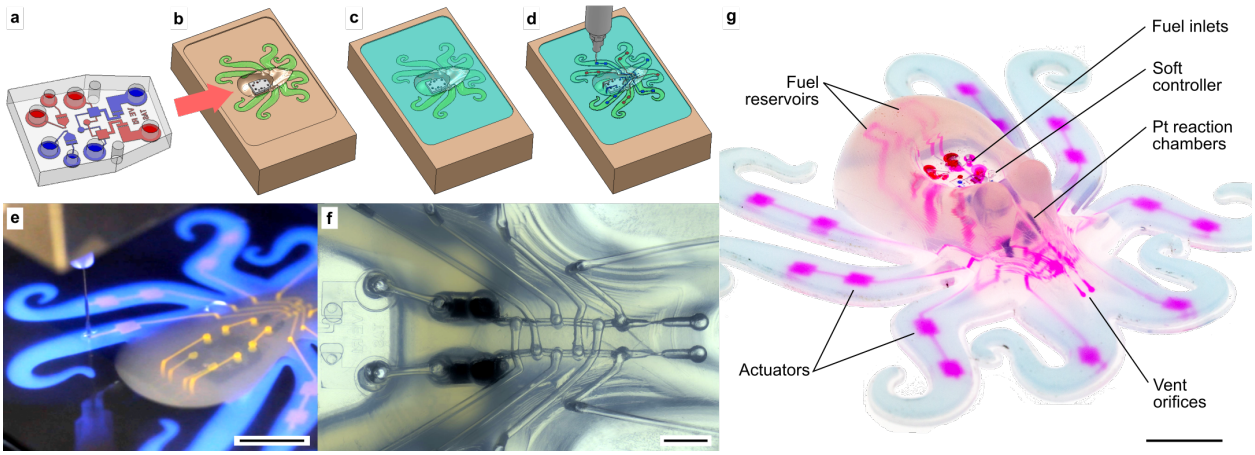

Figure 1. Fully soft, autonomous robot assembly. a, Pre-fabricate a microfluidic soft controller, and **b,** load this controller into a mold. **c,** Pour matrix materials into the mold and **d,e,** EMB3D print fugitive and catalytic inks (scale bar in **e** represents 10 mm). **f,** After matrix curing, the printed fugitive ink "auto-evacuates" yielding open channels (scale bar represents 2 mm). **g,** After curing, the octobot is removed from the mold and inverted to reveal an autonomous, fully soft robot, controlled via the embedded microfluidic soft controller and powered by monopropellant decomposition (scale bar represents 10 mm). Fluorescent dyes have been added in **e** and **g** to assist in visualization of internal features.

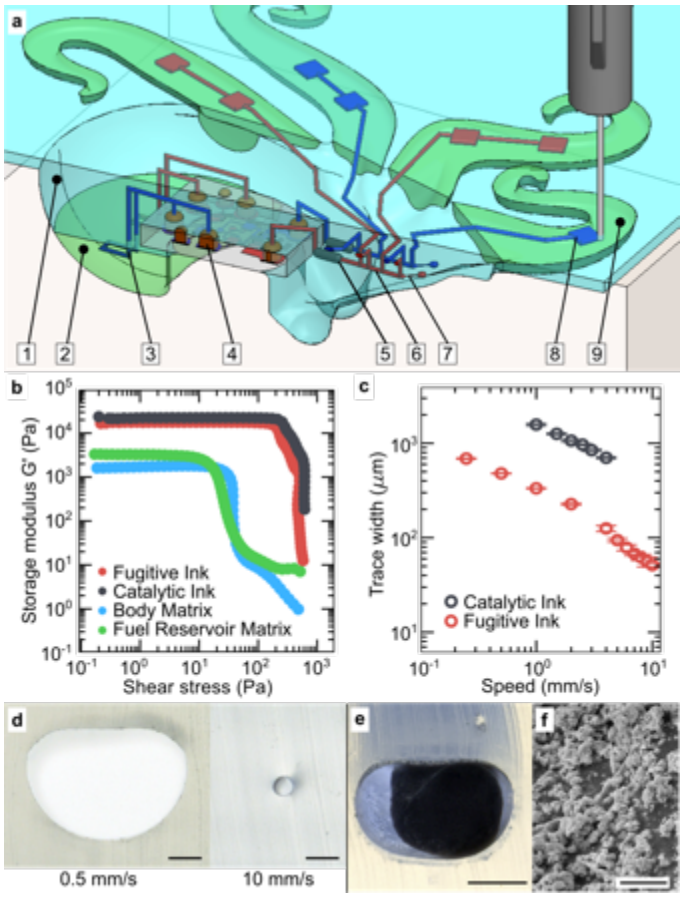

Figure 2. Multimaterial, EMB3D printing. a, The octobot features include (1) the body matrix, (2) fuel reservoir matrix, (3) printed fuel reservoir traces, (4) fugitive plugs in soft controller, (5) printed Pt reaction chamber, (6) printed pneumatic network, (7) printed vent orifices, (8) printed actuators, and (9) molded hyperelastic actuator matrix. All printed features are composed of the fugitive ink except (5), which is patterned using the catalytic ink. **b,** The storage modulus, G', of the fugitive ink, catalytic ink, body matrix, and fuel reservoir matrix is provided as a function of shear stress. The plateau storage moduli of the inks are an order of magnitude higher than those of the matrix materials. **c,** Trace widths of the fugitive and catalytic inks printed at 65 psi (450 kPa) and 50 psi (345 kPa), respectively, decrease with print speed (error bars indicate standard deviation). **d,** Optical images of channel cross-sections printed at speeds of 0.5 and 10 mm/s, which demonstrate that trace dimensions can be changed "on-the-fly" (scale bar is 100 mm). Reaction chambers printed with the catalytic inks containing a Pt-laden plug, as shown in **e,** a cross-section and **f,** scanning electron micrograph. (Scale bars in **e** and **f** represent 500 μm and 25 μm, respectively.)

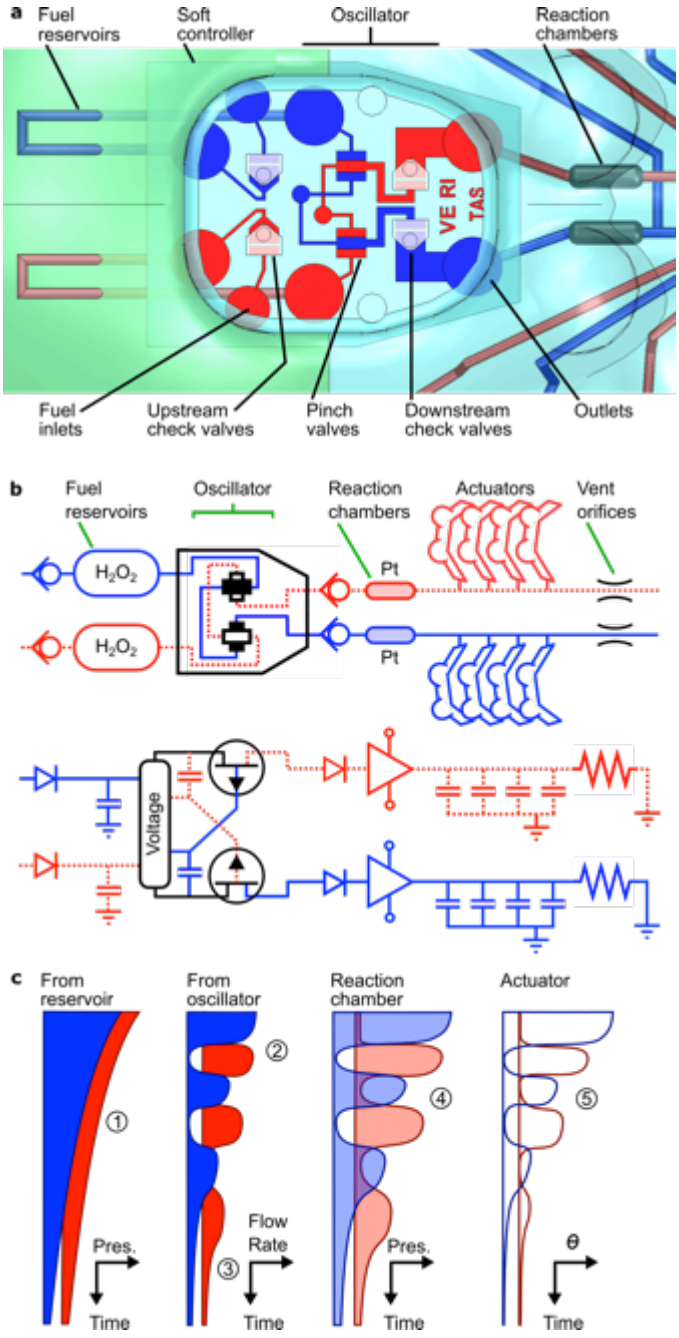

Figure 3. Octobot control logic. Discrete sides are shown in red and blue for clarity. **a,** A system of check valves and switch valves within the soft controller regulates fluid flow into and through the system. **b,** A schematic and qualitative electrical analogy of the octobot system are provided, where check valves, fuel tanks, oscillator, reaction chambers, actuators, and vent orifices are akin to diodes, supply capacitors, electrical oscillator, amplifiers, capacitors, and pull down resistors, respectively. **c,** Conceptual curves show key variables as a function of time. (1) Nominal pressure drives fuel through system at a decreasing rate. (2) Pinch valves in the oscillator convert upstream flow into alternating flow between red and blue channels. Flow rate and switching frequency are functions of upstream pressure and downstream impedance. (3) When upstream pressure is too low, oscillation is not possible, so both sides flow at reduced rate.

(4) Catalyst decomposes fuel, yielding pressurized gas, which flows downstream to the actuators and the vent orifices concurrently. (5) Actuators deform based on pressure. Vents must be sufficiently small to allow full actuation, yet sufficiently large to allow timely venting.

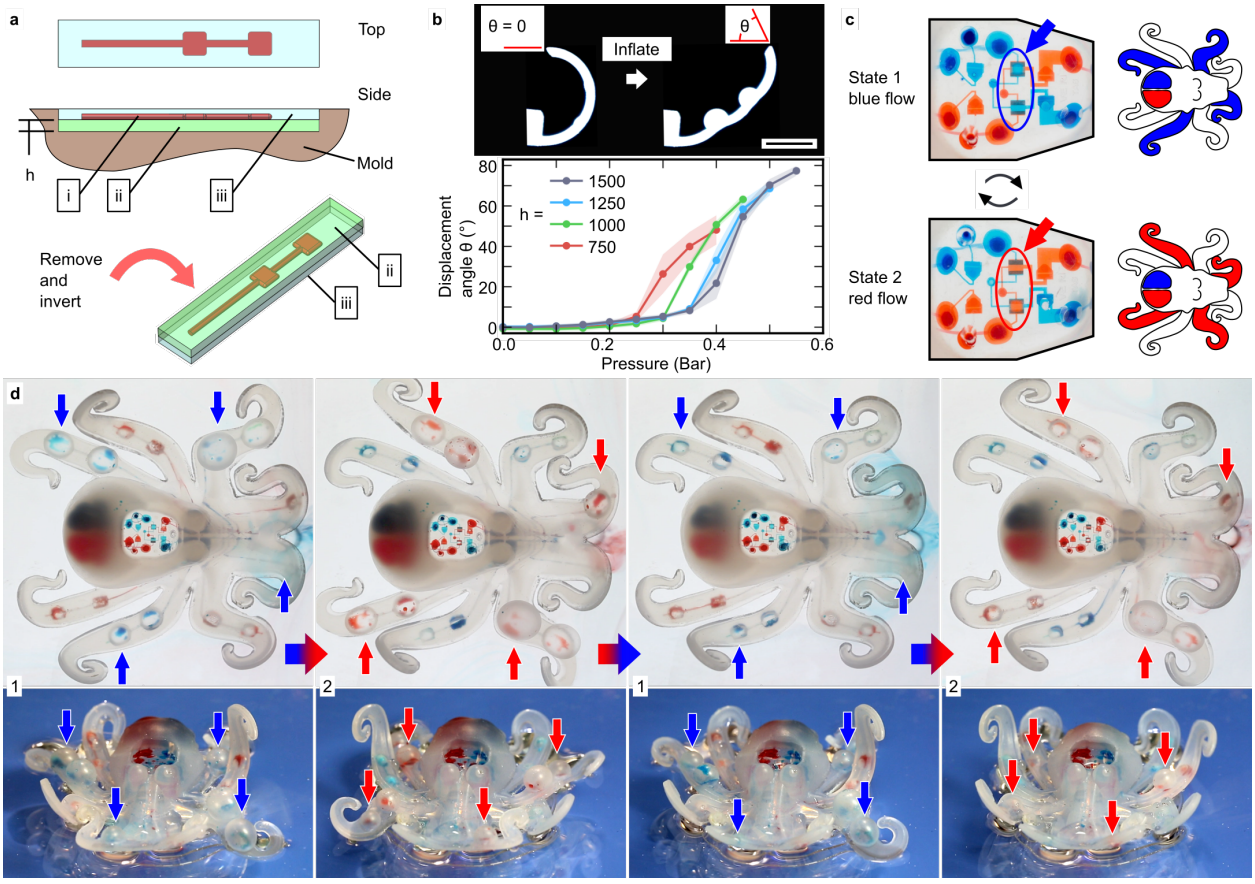

Figure 4. **Octobot actuation. a,** Actuator design in which traces (i) are printed in contact with the hyperelastic layer (ii) inside of the body matrix material and (iii) differences in modulus result in bending upon inflation. The thickness, *h*, of the hyperelastic layer is modified to change actuator characteristics. In this example, the body matrix material (iii) possesses a height of 800 μm. **b**, (Top) The actuator tip angle θ changes upon inflation (scale bar represents 10 mm). (Bottom) Displacement angle θ as a function of inflation pressure is provided for actuators with varying hyperelastic layer height, *h*, (in microns). Error bars indicate 95% confidence interval. **c,** The soft controller's oscillator causes an octobot to alternate between blue and red actuation states. The monopropellant fuel is dyed to show states. **d,** Stills from top-down (top) and face-on (bottom) operation videos show an octobot autonomously alternating between blue and red actuation states.

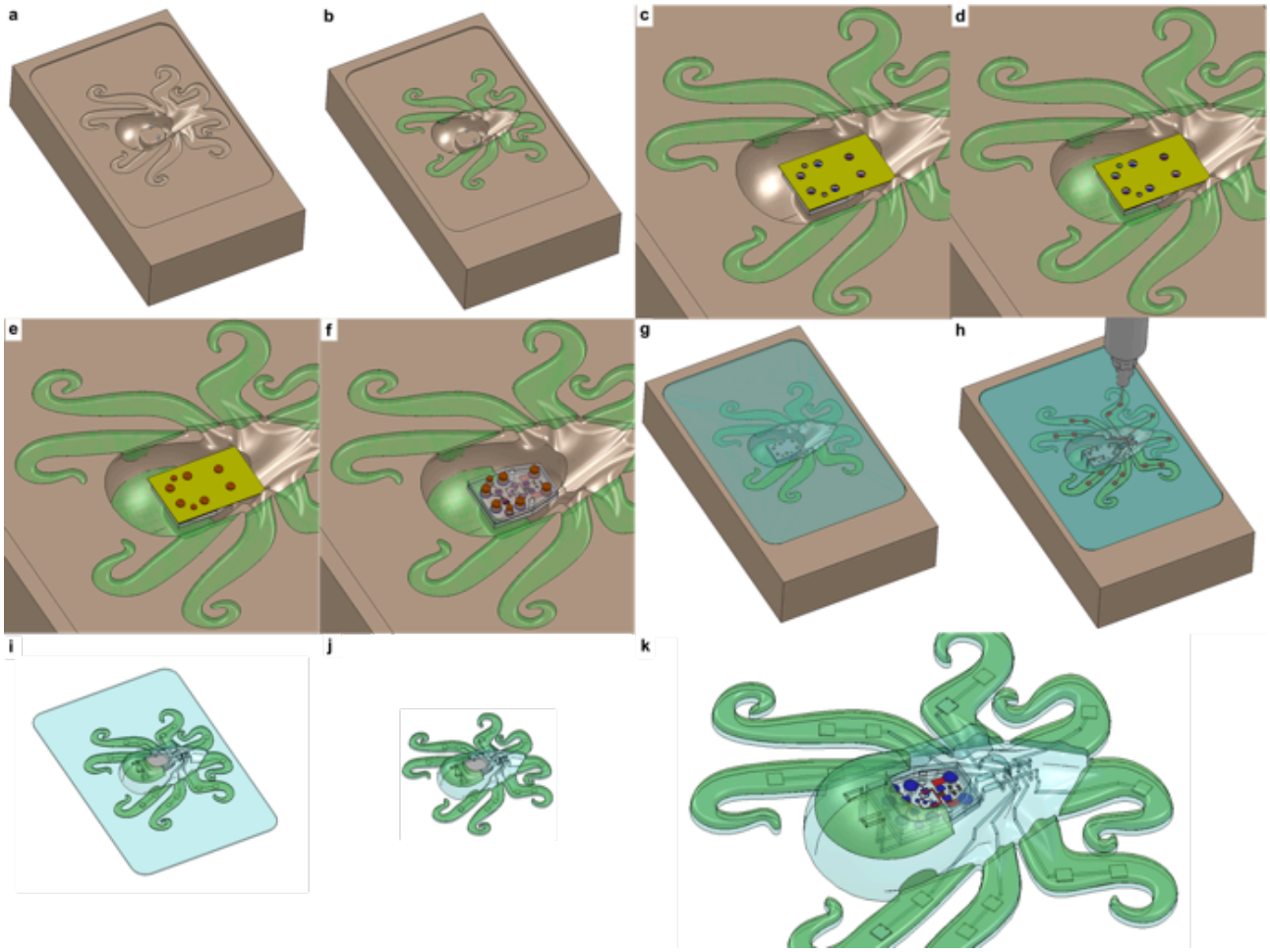

Extended Data Figure 1. Workflow for EMB3D printing an octobot. a, An EMB3D printing mold is machined from Delrin®. **b**, The hyperelastic layers needed for actuation are cast and crosslinked in the mold's actuator regions. **c,** A soft controller protected with a polyimide tape mask is loaded onto the EMB3D printing mold's pins. **d,** The fuel reservoir matrix material is carefully loaded into the fuel reservoir area of the mold and degassed under vacuum. **e**, Liquified fugitive plug material is manually loaded into the soft controller via the inlets and briefly degassed. **f,** The protective tape is removed after the fugitive plug material physically gels, and the fugitive plug is photocrosslinked. **g,** The body matrix material is cast into the mold and degassed. **h**, Any excess body matrix material is removed with a squeegee step, EMB3D printing begins, and the entire mold and EMB3D printed materials are placed in a 90˚C oven to crosslink. **i**, After two hours, the crosslinked octobot is removed from its mold and kept at 90˚C for a total of four days to ensure complete auto-evacuation of the aqueous fugitive inks. **j**, Before operation, excess body matrix material is removed via laser cutting. **k**, The final octobot, shown here in a close-up view, is prepared for operation.

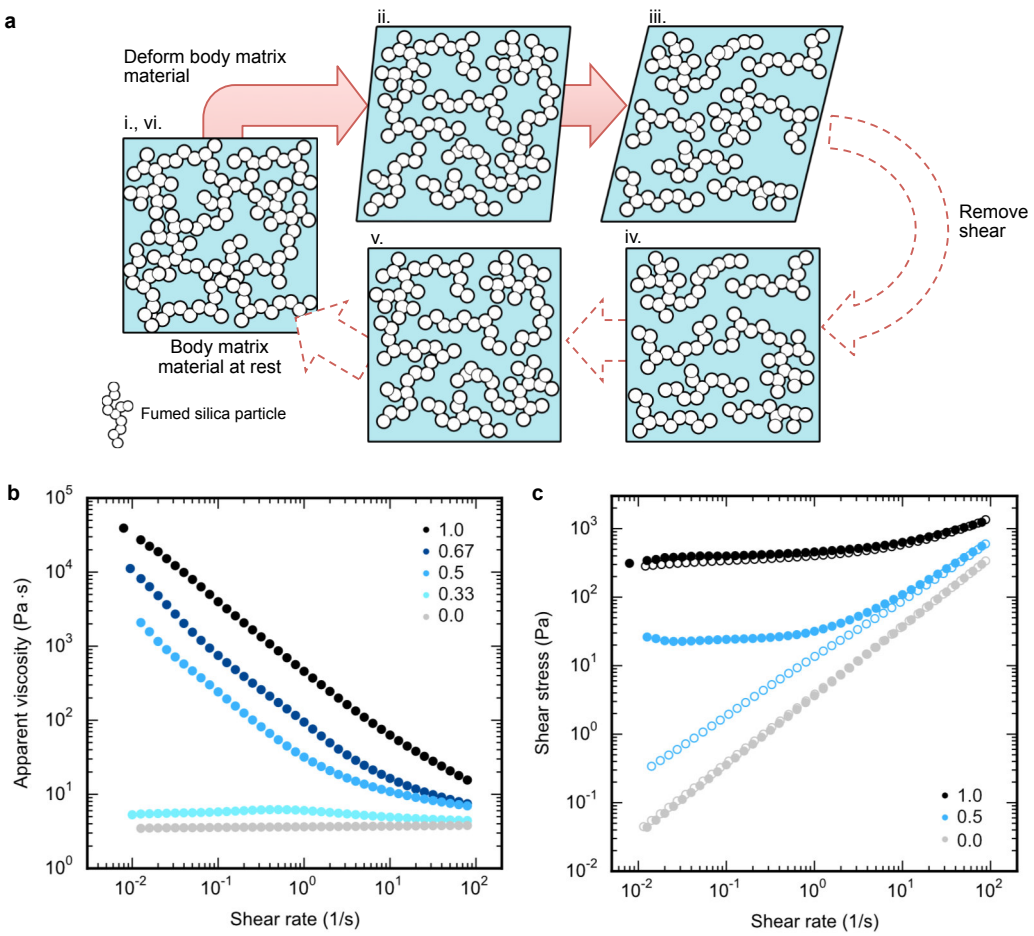

Extended Data Figure 2. Rheological properties of the body matrix. a, Schematic illustration of the body matrix behavior during the EMB3D printing process. (i) When the body matrix is at rest, the fumed silica fillers within the silicone material form a percolated network, which give rise to its shear yield stress, $\tau_{y,0}$. (ii) As nozzle travels through the matrix during printing, the matrix is yielded, and the percolated filler network is disrupted, which decreases the yield stress. (iii) Sufficient deformation can completely disrupt the fumed silica microstructure and completely eliminate the matrix material's yield stress ($\tau_{y,t} \rightarrow 0$ Pa). (iv) The fumed silica network does not immediately recover when it returns to a quiescent state. (v) Over time, the network slowly restructures to (vi) its equilibrium microstructure. **b,c,** Log-log plots of apparent viscosity (**b**) and corresponding shear stress versus shear rate (**c**) are shown for various PDMS matrix formulations investigated, which are prepared by blending Sylgard 184 (10:1 ratio of base to hardener) and SE 1700 (4:1 ratio of base to hardener) at various mass fractions. The formulations are listed by the weight ratio of SE 1700 used (0.0, 0.33, 0.5, 0.67, 1.0). **c,** Closed and open circles in the plot represent measurements taken during the flow sweep and ramp steps of the thixotropic loop studies, respectively. The final body matrix, formulated from the 50 wt% SE 1700 blend, shows clear thixotropic behavior and a significant decrease in yield stress upon yielding. Blends with higher concentrations of filler particles show diminished thixotropic behavior, and the yield stress is not eliminated during nozzle translation. Consequently, crevices or air pockets form during printing with matrix materials possessing higher concentrations of fumed silica.

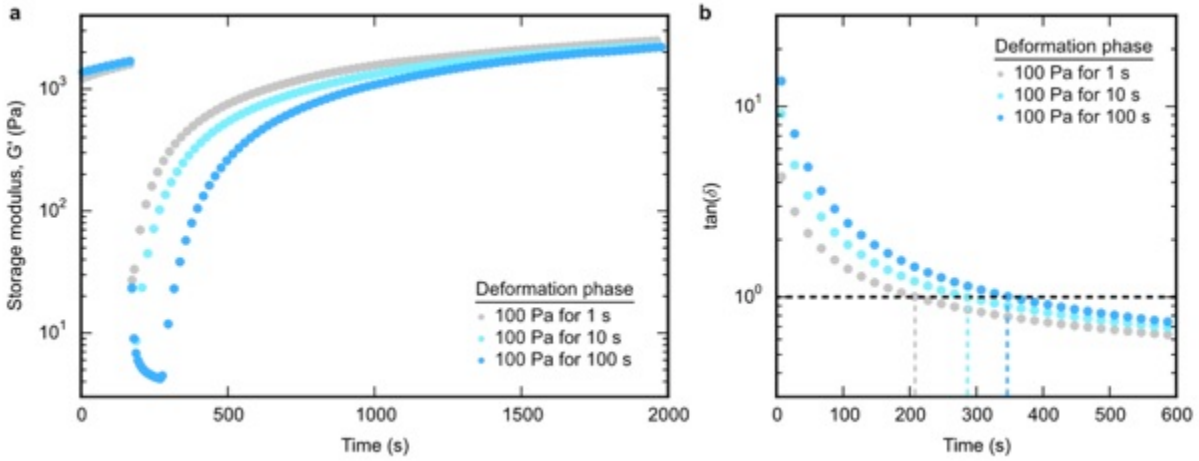

Extended Data Figure 3. Modulus recovery of the body matrix after yielding. a, A plot of storage modulus (G') as a function of time illustrates how the body matrix's modulus recovers during three-phase thixotropy tests. After a probe phase, a shear stress of 100 Pa is applied for varying times during a deformation phase, resulting in temporary fluidization of the matrix material. During the recovery phase, the modulus increases over time. **b**, tan(δ), the ratio of the loss modulus (G'') to the storage modulus (G'), is plotted as a function time for each of the recovery phases measured in **a**. Onset of recovery of the body matrix material's yield stress – and the onset of fumed silica filler percolation in a recovering matrix material – is assumed to be the moment $G' = G''$, or tan(δ) = 1. Thus, the body matrix material's "recovery time" is approximately the time at which tan(δ) = 1 after deformation. Since the momentary deformation incurred by nozzle translation through a discrete volume of matrix material during EMB3D printing happens within a time period shorter than 1 s and with a magnitude less than 100 Pa, the body matrix material's thixotropic recovery time is less than 200 s, the approximate time it takes the body matrix to recover after sheared by a 100 Pa stress for 1 s.

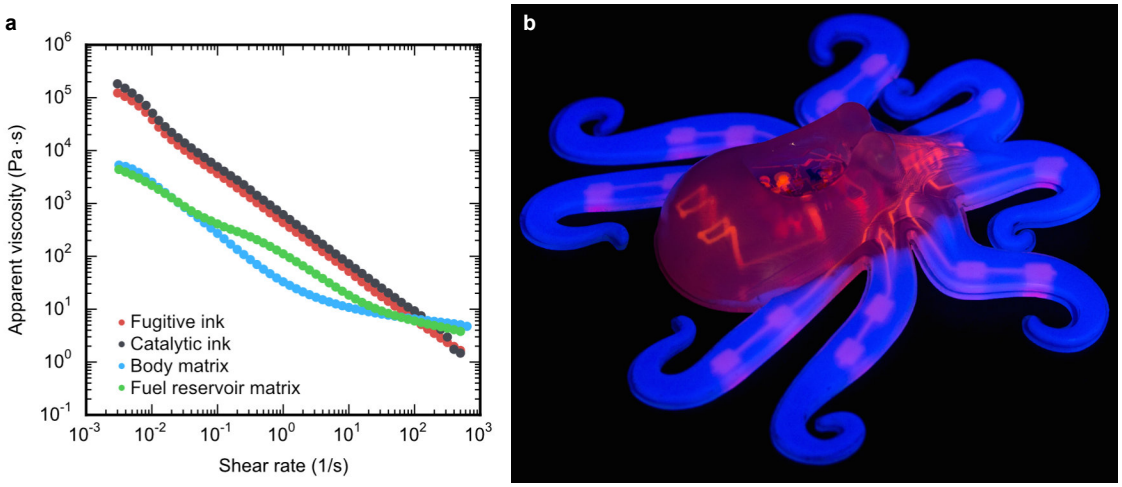

Extended Data Figure 4. Rheological and printing behavior of inks and matrix materials used to fabricate an Octobot. **a,** A log-log plot of apparent viscosity as a function of shear rate is provided for the fugitive ink (red), catalytic ink (black), body matrix material (blue), and fuel reservoir matrix material (green). **b,** An octobot with fluorescently dyed fugitive inks (red, not auto-evacuated) and hyperelastic actuator layers (blue) fabricated by molding and EMB3D printing.

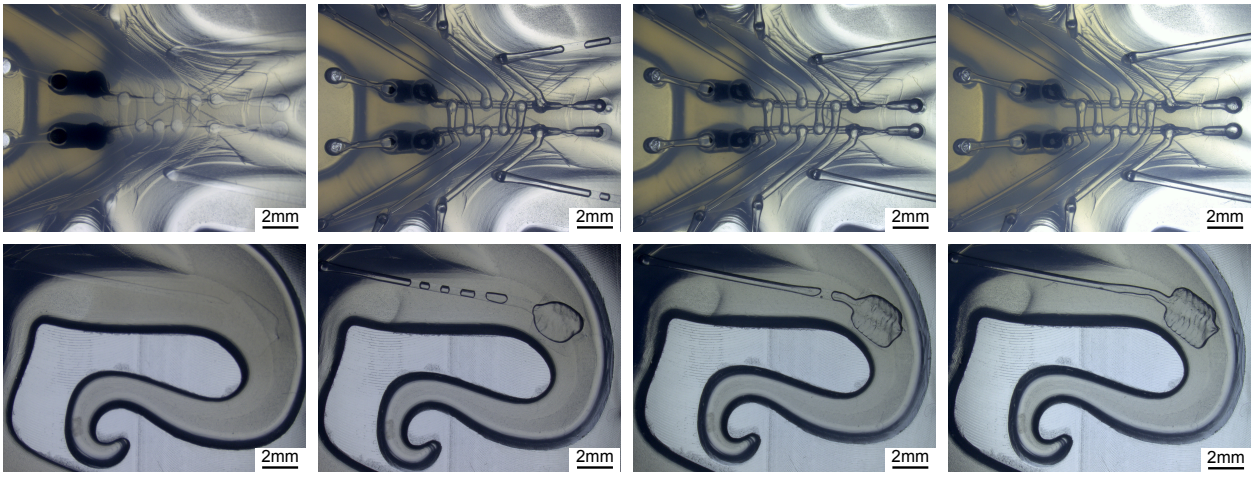

Extended Data Figure 5. Auto-evacuation of the fugitive and catalytic inks. Photographs of an octobot's reaction chambers with upstream portions of the actuator networks (top) and a one-pad actuator at various times, *t*, reveal the auto-evacuation of the fugitive and catalytic inks, which leaves behind open channels that serve as mesofluidic features

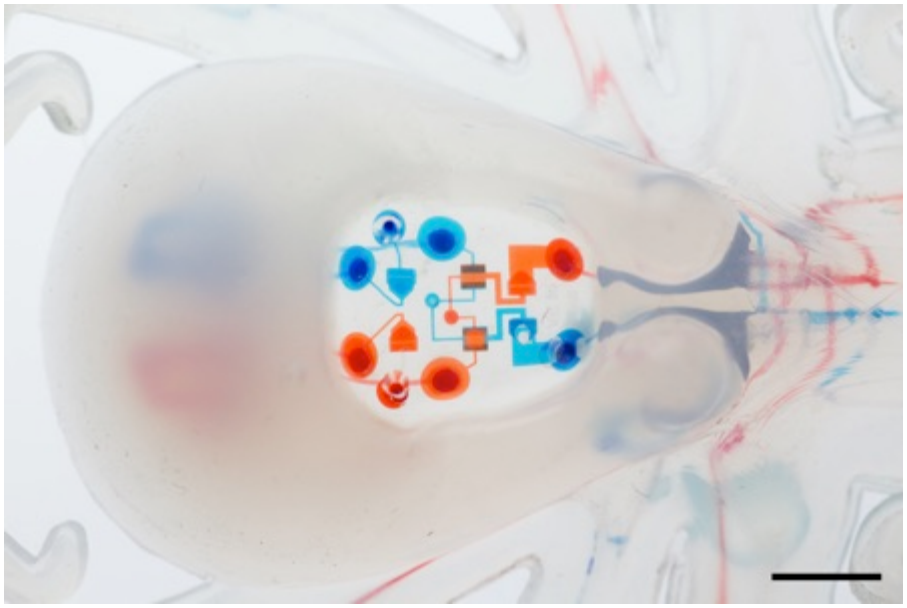

Extended Data Figure 6. Infilling the soft controller from the fuel inlets. Water (with red or blue dye) is introduced into the fuel reservoir via the fuel inlets. Continuity between the fuel reservoirs, soft controller, and downstream EMB3D printed components is possible because of the fugitive plugs, which auto-evacuate along with the EMB3D printed inks. (The scale bar indicates a length of 5 mm.)

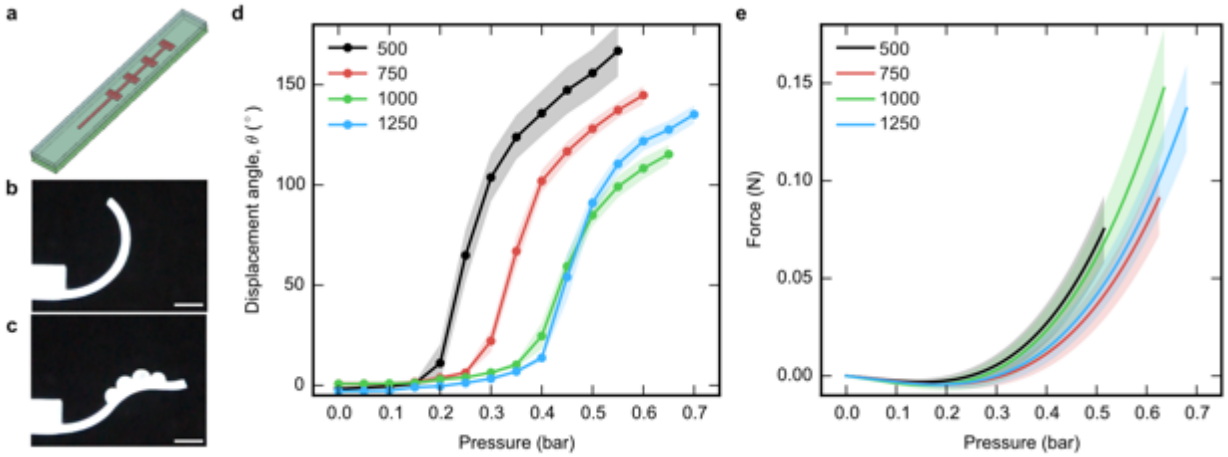

Extended Data Figure 7. Characterization of EMB3D printed actuators. a, CAD model of a four-bladder actuator design. Other bladder number, the design is similar to the actuators illustrated in Figure 4a. **b,** EMB3D printed actuator is shown prior to inflation. **c,** Actuator inflated to working pressure. (Scale bars in **b** and **c** indicate 5 mm.) **d,** Pressure versus displacement curves for four-bladder actuators with varying thickness of hyperelastic layer. **e,** Pressure versus force curves varying thickness of hyperelastic layer. (For **d** and **e**, thicknesses of the hyperelastic layer shown are in µm. Shaded regions indicate 95% confidence interval.) Detailed procedures for characterizing actuator performance are provided in the Methods.

Table S1. Break-in and working gauge pressures for EMB3D printed actuators.

	Two bladder actuators		Four bladder actuators	
Hyperelastic layer thickness (mm)	P_0 (Bar)	P_1 (Bar)	P_0 (Bar)	P_1 (Bar)
500	0.35	0.3	0.6	0.55
750	0.4	0.35	0.65	0.6
1000	0.45	0.4	0.7	0.65
1250	0.5	0.45	0.75	0.7
500	0.55	0.5	0.8	.075

List of Supplementary Videos and Tables

Supporting Video 1. EMB3D printing of an octobot.

Supporting Video 2. Decomposition of monopropellant fuel in the presence of catalyst.

Supporting Video 3. Octobot operation demo (front view).

Supporting Video 4. Octobot operation demo (top down view).

Table S1. Break in and working gauge pressures for EMB3D actuators.